Letter

Topological Kondo model out of equilibrium

Matteo M. Wauters [1,2] Chia-Min Chung [3,4,5] Lorenzo Maffi [1] and Michele Burrello [1]

[1] *Niels Bohr International Academy and Center for Quantum Devices, Niels Bohr Institute, Copenhagen University, Universitetsparken 5, 2100 Copenhagen, Denmark*

[2] *Pitaevskii BEC Center, Department of Physics, University of Trento, Via Sommarive 14, I-38123 Povo, Trento, Italy*

[3] *Department of Physics, National Sun Yat-sen University, Kaohsiung 80424, Taiwan*

[4] *Center for Theoretical and Computational Physics, National Sun Yat-Sen University, Kaohsiung 80424, Taiwan*

[5] *Physics Division, National Center for Theoretical Sciences, Taipei 10617, Taiwan*

(Received 14 July 2023; revised 20 November 2023; accepted 22 November 2023; published 18 December 2023)

The topological Kondo effect is a genuine manifestation of the nonlocality of Majorana modes. We investigate its out-of-equilibrium signatures in a model with a Cooper-pair box hosting four of these topological modes, each connected to a metallic lead. Through an advanced matrix-product-state approach tailored to study the dynamics of superconductors, we simulate the relaxation of the Majorana magnetization, which allows us to determine the related Kondo temperature, and we analyze the onset of electric transport after a quantum quench of a lead voltage. Our results apply to Majorana Cooper-pair boxes fabricated in double nanowire devices and provide nonperturbative evidence of the crossover from weak-coupling states to the strongly correlated topological Kondo regime. The latter dominates at the superconductor charge degeneracy points and displays the expected universal fractional zero-bias conductance.

DOI: 10.1103/PhysRevB.108.L220302

The engineering of Majorana zero-energy modes (MZMs) in hybrid superconducting-semiconducting devices has been the core of strenuous theoretical and experimental activities for the last two decades [1–3]. The detection of these subgap modes relies primarily on tunneling spectroscopy applied to a rich variety of platforms, which, however, cannot provide direct evidence of the most intriguing properties of MZMs, namely their nonlocal and anyonic features. Hence, it is desirable to devise a new generation of experiments that balances the constraints imposed by the current technological limitations and the pursuit of MZM evidence beyond spectroscopy.

In this respect, the topological Kondo effect (TKE) [4–6] plays a crucial role: on one side, it is a transport signature of MZMs well-suited for experimental observations; on the other, it results from their nonlocality and can hardly be confused with phenomena originating by nontopological subgap states [7]. The TKE is predicted to emerge in multiterminal devices where M external leads are coupled to a Majorana Cooper-pair box hosting four MZMs and characterized by a charging energy E_c (Fig. 1). The TKE manifests itself as a universal nonlocal zero-bias conductance $dI_\alpha/dV_{\beta\neq\alpha}$ quantized at values $2e^2/Mh$. Such conductance is approached at low temperatures in correspondence of both the Coulomb valleys and peaks of the related devices [8], as derived from renormalization group (RG) analyses of effective low-energy models describing the Majorana Cooper-pair box coupled to M leads [4–6,8–12].

In this Letter, we address the experimental observability of the TKE from a more elementary and microscopic perspective and we examine its onset out of equilibrium. We characterize the quantum-quench dynamics of a minimal interacting fermionic model that includes both MZMs and quasiparticle excitations above the superconducting gap. The time evolution is determined by electrons tunneling from the leads to the superconducting (SC) island, and, differently from previous TKE studies [4,6,10,13–16], we apply matrix-product-state (MPS) simulations [17] which do not rely on any perturbative approximation of this coupling or on a clear energy scale separation. This technique allows us to examine the crossover between the predicted weak-coupling and topological Kondo strong-coupling regimes and estimate the related topological Kondo temperature T_K.

The model we propose provides a minimal description of Majorana Cooper-pair boxes engineered from nanowires. Recent developments in the fabrication of parallel InAs nanowires hybridized with Al [18,19] make these platforms suitable to combine all the necessary elements to implement the topological Kondo model. It is therefore important to investigate its transport signatures as a function of the most relevant experimental parameters: lead voltages, charge induced on the SC island, and lead-island couplings.

Model and methods. We consider a TKE model composed by two parallel 1D topological superconductors coupled by a common floating SC island with charging energy E_c and charge n_g induced by the potential V_g (Fig. 1). It describes two nanowires with strong spin-orbit coupling subject to a proximity-induced SC pairing and a suitable Zeeman interaction, which provide a common route to engineer MZMs [20,21]. Their low-energy physics is captured by spinless fermions subject to an emergent p-wave SC pairing Δ_P. As a result, four MZMs $\{\gamma_\alpha\}_{\alpha=1,\dots,4}$ form at the nanowire edges, each coupled to a spinless normal lead. The tunneling rates Γ_α between leads and MZMs can be switched off to change the number of terminals $M \leqslant 4$ coupled to the system.

The simplest description for each SC nanowire is a zero-bandwidth model [22–24], where the lowest energy level is

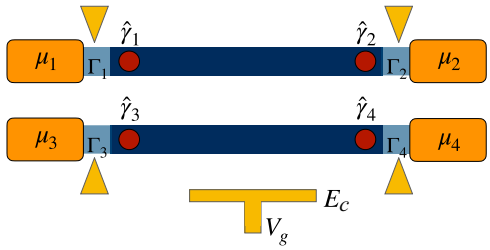

FIG. 1. Schematics of the system: Two p-wave superconducting nanowires with MZMs at the edges are coupled by a SC island (blue) with charging energy E_c. Voltage gates (yellow) tune the island-induced charge, $n_g \propto V_g$, and the coupling rates Γ_α with the leads (orange). Each MZM is coupled with a single normal lead at chemical potential μ_α.

the subgap state defined by two Majorana operators, while the higher energy state represents Bogoliubov quasiparticles above the SC gap. This corresponds to a 2-site Kitaev chain for each nanowire, with each of the four constituting fermionic sites tunnel-coupled to one of the leads. This system defines the SC box sketched in Fig. 1, with Hamiltonian $\widehat{H} = \widehat{H}_{\rm sys} + \widehat{H}_L + \widehat{H}_{\rm t}$. $\widehat{H}_{\rm sys}$ describes the Majorana Cooper-pair box [25,26]:

$$\widehat{H}_{\rm sys} = \sum_{\sigma,n} \epsilon_{n,\sigma} \hat{f}^\dagger_{n,\sigma} \hat{f}_{n,\sigma} + E_c(\hat{N} - n_g)^2, \tag{1}$$

where $\sigma = \uparrow, \downarrow$ labels the upper and lower nanowires and $n = 0, 1$ the two quasiparticle states in each of them [27]. $\hat{N}$ is the total box charge with respect to an arbitrary offset. It includes both its Cooper pairs and the electrons in the nanowires.

The two zero-energy quasiparticles are generated by the combinations of MZMs $\hat{f}_{0,\uparrow} = (\hat{\gamma}_1 - i\hat{\gamma}_2)/2$ and $\hat{f}_{0,\downarrow} = (\hat{\gamma}_3 - i\hat{\gamma}_4)/2$. We label the four corresponding low-energy states by $|n_\uparrow n_\downarrow\rangle$, with $\hat{n}_\sigma = \hat{f}^\dagger_{0,\sigma}\hat{f}_{0,\sigma}$. The charging energy splits them into two degenerate pairs with different fermionic parity $(-1)^{\hat{N}}$. Hereafter, we set equal SC pairing and nanowire hopping, $\Delta_P = t_{\rm sys} = 0.5t_0$, and introduce a small potential $\mu_{\rm sys} = 0.01t_0$ [27].

The leads are modeled by Wilson chains [17,28,29]

$$\widehat{H}_L = \sum_{\alpha=1}^{4}\sum_{l=1}^{\mathcal{L}} [-t_0 e^{-(l-1)/\xi} \hat{c}^\dagger_{\alpha,l+1}\hat{c}_{\alpha,l} + \text{H.c.}] - \mu_\alpha \hat{c}^\dagger_{\alpha,l}\hat{c}_{\alpha,l}, \tag{2}$$

with t_0 being the *bare* hopping amplitude which sets their bandwidth and constitutes the largest energy scale. The hopping decay length ξ is an auxiliary variable allowing us to tune the resolution at small energies by modifying the lead level spacing [17,29,30]. The chemical potentials μ_α are used to bring the system out of equilibrium and study transport properties.

The tunneling Hamiltonian between the leads and the system is

$$\widehat{H}_{\rm t} = -\sum_{\alpha=1}^{4}\sum_{\sigma,n} J_\alpha[(u_{\alpha,\sigma,n}\hat{f}^\dagger_{\sigma,n} + v_{\alpha,\sigma,n}\hat{f}_{\sigma,n})\hat{c}_{\alpha,1} + \text{H.c.}], \tag{3}$$

where $u_{\alpha,\sigma,n}$ ($v_{\alpha,\sigma,n}$) is the particle (hole) projection of $\hat{f}_{\sigma,n}$ on the real-space site coupled to lead α. The amplitudes J_α determine the effective tunneling rates $\Gamma_\alpha = \frac{J_\alpha^2}{2t_0}$.

In our simulations, we map the system into an MPS by following Refs. [17,30]. Each MPS site represents a single-particle eigenstate of either the leads or the nanowires (Bogoliubov quasiparticles for nanowires) and we order them based on their energy. The charge $\hat{N}$ is encoded in an auxiliary site [27,31]. The real-time dynamics is simulated using the time-dependent variational principle algorithm [32–34] from the ITensor library [35,36]. We set the MPS truncation error $\sim 5 \times 10^{-8}$, corresponding to a maximum bond dimension $\chi \lesssim 2000$.

Relaxation toward equilibrium. In the Kondo problem dynamics, the formation of strong correlations and the Kondo screening cloud occur over a timescale given by T_K^{-1} [30,37–39]. Therefore, the relaxation after a quantum quench offers a useful probe to estimate the Kondo temperature and detect strongly correlated states.

In the following, we consider the dynamics of the system in a postquench nonequilibrium quasisteady state (NEQSS). In this regime, the time evolution fulfills a Lieb-Robinson bound [40,41] such that the dynamics is not affected by finite-size limitations until the signal propagates to the edge of the simulated system. Due to this, the information acquired from the analysis of the NEQSS well represents the out-of-equilibrium physics in the thermodynamic system (see, for instance, Refs. [42–45]), as verified also by applying our protocol to superconducting interacting scatterers [17] and the Anderson impurity model [30].

The first quench protocol we consider aims at observing the relaxation of the Majorana Cooper-pair box caused by $\widehat{H}_{\rm t}$. The box is initialized in the ground state $|00\rangle$ ($N = 0$ for $n_g < 0.5$) or $|10\rangle$ ($N = 1$ for $n_g > 0.5$) and is decoupled from the leads, which are set at half filling. At time $t = 0$, the couplings Γ are suddenly turned on and the device begins relaxing toward equilibrium. To characterize this relaxation, we analyze the average island charge $\langle\hat{N}(t)\rangle$ and the effective Majorana magnetization [4,13] $\langle\hat{Z}_{\rm eff}(t)\rangle \equiv \langle i\hat{\gamma}_3\,\hat{\gamma}_4(t)\rangle = 1 - 2\langle\hat{n}_\downarrow(t)\rangle$.

The observed dependence of $\langle\hat{N}\rangle$ on n_g after equilibration (Fig. 2) shows the crossover between the weak-coupling and the strong-coupling regime. Following Ref. [46], we characterize the weak-coupling regime at $n_g \sim 0$ by the slope of $\langle\hat{N}\rangle = \frac{M\Delta_P\Gamma}{E_c t_0} n_g$: For weak Γ, the charge data sets corresponding to different choices of E_c and M [47] exhibit a good agreement with the expected linear dependence [inset of Fig. 2(a)]. On the other hand, the sinusoidal correction derived for the strong-coupling regime [46],

$$\langle\hat{N}\rangle = n_g - \left(\frac{E_c}{\Delta_P}\sqrt{1 - \Gamma/t_0}\right)^M \sin(2\pi n_g), \tag{4}$$

closely matches the numerical data for the highest value of the tunneling rate $\Gamma = 0.08t_0$ [gray dot-dashed line and red squares in Fig. 2(a)], thus suggesting the emergence of Kondo correlations.

Importantly, the relaxation timescale of $\langle\hat{N}\rangle$ depends on the ratio Γ/E_c but not on the induced charge n_g, as shown in Fig. 2(b) which displays the time dependence of the relative

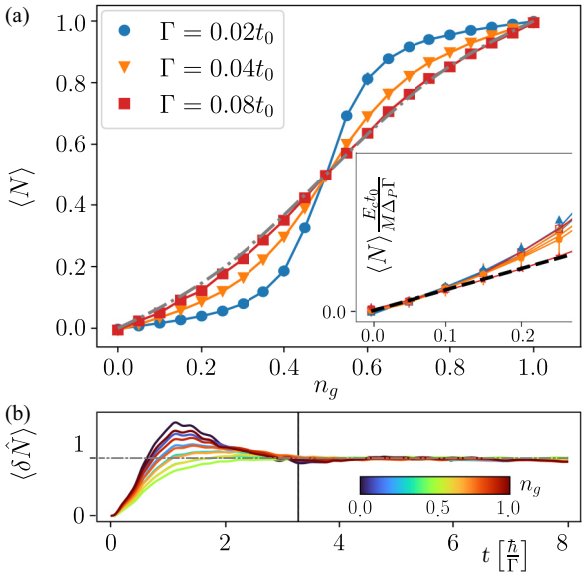

FIG. 2. (a) Equilibrium charge versus n_g, for $M = 3$, $E_c = 0.2t_0$. The gray dot-dashed line corresponds to Eq. (4) for $\Gamma = 0.08t_0$. Inset: Data for different values of E_c ($0.2t_0$ and $0.4t_0$) and $M = 3$, 4 in the weak-coupling regime, rescaled by $\frac{M\Delta_P\Gamma}{E_c t_0}$. The dashed black line corresponds to $\langle \hat{N} \rangle = \frac{M\Delta_P\Gamma}{E_c t_0} n_g$. (b) Charge relaxation for different values of $n_g \in [0, 1]$, $E_c = 0.2t_0$, and $\Gamma = 0.04t_0$. All data are obtained with $\mathcal{L} = 64$ and $\xi = 16$.

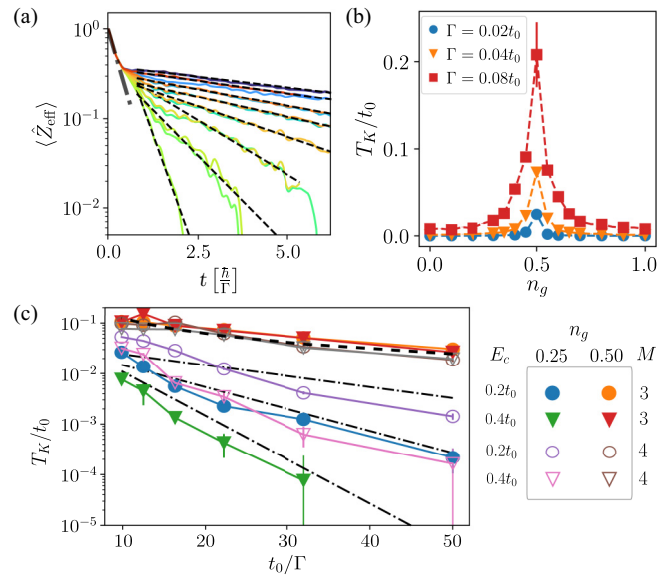

FIG. 3. (a) Dynamics of the Majorana magnetization for different values of $n_g \in [0, 1]$; $E_c = 0.2t_0$ and $\Gamma = 0.08t_0$. The dot-dashed line marks the decay rate Γ. (b) T_K extracted as the relaxation rate of $\langle \hat{Z}_{\rm eff} \rangle$—dashed lines in panel (a)—as a function of n_g. (c) T_K as a function of t_0/Γ at $n_g = 0.5$ and in the even-parity Coulomb valley ($n_g = 0.25$). Dot-dashed lines correspond to Eq. (6), whereas the dashed line marks the degeneracy point scaling $T_K \sim M\Gamma$. A prefactor $C \sim 0.2$ has been manually set to approximately match the data. All data are obtained with $\mathcal{L} = 64$, $\xi = 16$.

charge variation,

$$\langle \delta \hat{N}(t) \rangle = \frac{|\langle \hat{N}(t) \rangle - \langle \hat{N}(0) \rangle|}{|\langle \hat{N}(t \to \infty) \rangle - \langle \hat{N}(0) \rangle|}. \tag{5}$$

The vertical line marks the equilibration time, and different curves, corresponding to different values of $n_g \in [0, 1]$, converge to $\langle \delta \hat{N}(t) \rangle = 1$ on similar timescales.

The magnetization, instead, displays a remarkably different behavior [Fig. 3(a)]. At short times, $t < \hbar/\Gamma$, the relaxation is dominated by the fast rate Γ (dot-dashed line) independently of both E_c and n_g. Then, a second timescale emerges, which depends on both Γ and the energy difference $\delta E(n_g) = E_c|1 - 2n_g|$ between the charge sectors $N = 0$ and $N = 1$. The black dashed lines in Fig. 3(a) are exponential fits of these slower decays. This behavior is analogous to the magnetization relaxation in the Anderson impurity model [30,38,48], suggesting that this longer timescale is associated with the energy scale T_K of the emerging TKE.

The comparison of Figs. 3(a) and 2(b) underlines that this Kondo timescale characterizes only the Majorana magnetization but not the charge; $\langle \hat{Z}_{\rm eff} \rangle$ constitutes indeed one of the effective Pauli operators at the heart of the definition of the TKE, whereas $\langle \hat{N} \rangle$ depends only on the fermionic parity of the SC island. Therefore, we interpret this charge-"spin" separation as evidence of the TKE emergence.

Next, we analyze the dependence of the so-derived T_K on n_g, Γ, and E_c. Figure 3(b) depicts the fitted T_K as a function of n_g for different values of Γ and $E_c = 0.2t_0$. As expected from RG analyses, T_K is larger at the charge degeneracy point where it is proportional to $M\Gamma$, consistently with Ref. [46]. In the Coulomb valleys, instead, T_K is qualitatively compatible with standard RG predictions [46]:

$$T_K \sim E_c e^{-\frac{\delta E(n_g) t_0}{2(M-2)\Gamma\Delta_P}}. \tag{6}$$

The different behaviors at the charge degeneracy point ($n_g = 0.5$) and in the even Coulomb valley ($n_g = 0.25$) are exemplified in Fig. 3(c), which displays T_K versus t_0/Γ for two values of E_c and M (see legend). T_K extracted at $n_g = 0.5$ is independent of both E_c and M and it decreases with a power law compatible with $T_K \sim \Gamma$ (dashed line). For large values of Γ, the magnetization can change sign, preventing us from extracting T_K with high precision [see the large error bar at $n_g = 0.5$ in Fig. 3(b)]. In the Coulomb valleys, instead, T_K shows a substantial drop when increasing E_c: not only is it smaller for $E_c = 0.4t_0$, but it decreases faster with $1/\Gamma$, in accordance with Eq. (6) (dot-dashed lines). The data for $M = 4$, $E_c = 0.4t_0$ and $M = 3$, $E_c = 0.2t_0$ almost coincide as Eq. (6) predicts the same behavior but for a factor 2 in front. Our data display a concavity that is absent in Eq. (6) and suggests a competing power-law dependence on Γ in agreement with NRG results of the low-energy effective model [10]. The presence of a power-law correction can also be understood as the interpolation between the scaling of T_K deep in the Coulomb valleys, where it is dominated by the exponential decay, and that at $n_g = 0.5$, where it is proportional to Γ. At intermediate values of the induced charge, $0 < n_g < 0.5$, we expect a gradual crossover between the two regimes when the coupling strength Γ becomes comparable with the charge excitations, as either Γ increases or the charge degeneracy point is approached.

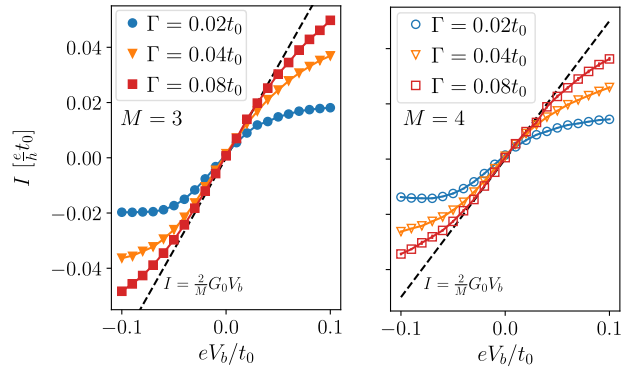

FIG. 4. Average nonlocal current versus V_b at $n_g = 0.5$, for $M = 3, 4$. The dashed line highlights the TKE prediction $G = \frac{2}{M}G_0$. The data are obtained with $\mathcal{L} = 100$ and $\xi = 32$.

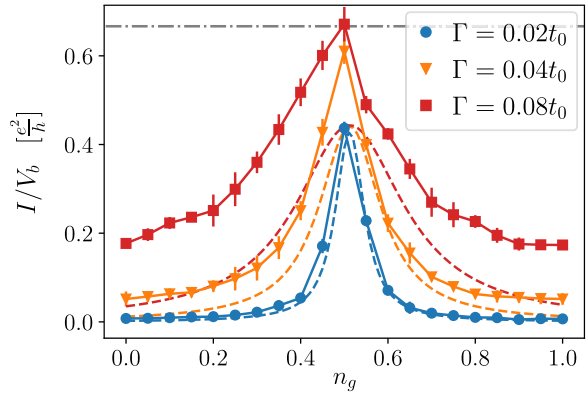

FIG. 5. Nonlocal current versus n_g, for $E_c = 0.4t_0$. The dashed lines are the corresponding RL approximation [27]. The horizontal dot-dashed line is $\frac{2e^2}{hM}$ with $M = 3$.

Nonlocal transport. To investigate multiterminal transport properties, we adopt a different quench protocol, using DMRG to prepare the ground state of the device coupled with M leads at equilibrium ($\mu_\alpha = 0$). In general, such a state is a superposition of different charge and magnetization states. At $t = 0$ we quench the chemical potential in the first lead to a finite value $\mu_1 = eV_b$ and compute the average current flowing through the remaining connected terminals. We refer to the latter as average nonlocal current.

RG predicts a fractional zero-bias nonlocal conductance, $G_{\mathrm{TKE}} = \frac{2}{M}\frac{e^2}{h}$, independent from all other physical parameters for $T \ll T_K$, both in the Coulomb valleys [4–6] and at the charge-degeneracy points [8,11,16,46]. Our simulations capture this fractional conductance for $M = 3, 4$ for sufficiently strong coupling in proximity of $n_g = 0.5$, where T_K is maximum and G_{TKE} can be observed for an extended voltage bias window (Fig. 4). For $n_g \sim 0.5$, we also observe non-Fermi-liquid power-law corrections with non-integer exponents which, however, do not seem compatible with the first-order scaling predicted by bosonization and RG [8,11,15,16,27,46,49].

Our simulations are performed at zero temperature, but, away from $n_g = 0.5$, T_K becomes comparable with the energy we introduce with the finite bias eV_b, competing with the universal strong-coupling features of the model. In Fig. 5 we plot the average nonlocal current ($M = 3$ and $E_c = 0.4t_0$) divided by the voltage bias as a function of n_g. We set $\mu_1 = eV_b = 0.02t_0$, which is small enough to probe the response close to the linear regime, yet the data display a good signal-to-noise ratio. The TKE prediction is met at the charge degeneracy point and strong coupling, consistently with Fig. 4, while the strong n_g dependence confirms that we are not deep in the TKE regime; however, several hints of a strongly correlated Kondo state emerge also in the Coulomb valleys.

In Fig. 5, we compare our data with the conductance G_{RL} of a single fermionic resonant level (RL), which exhibits a peak scaling as $4G_0/M^2$ with width $\sim M\Gamma/E_c$ (dashed lines) [27]. The data with the weakest coupling ($\Gamma = 0.02t_0$) match well the RL approximation, as expected in a weak-coupling regime. By increasing Γ, we observe large deviations from the single RL and the conductance rapidly approaches the TKE value of $\frac{2}{3}G_0$ (horizontal dot-dashed line) for $n_g \sim 0.5$. Indeed, in this regime, the applied voltage $\mu_1 = 0.02t_0$ is one order of magnitude smaller than the estimate of the Kondo temperature, $T_K \sim 0.1t_0$, in Fig. 3(c). Moreover, there is a substantial current flowing deep in the Coulomb valleys ($\Gamma = 0.08t_0, 0.04t_0$) with apparent plateaus that suggest a crossover to the TKE regime. This is further confirmed by the analysis of the data averaged over the decay length ξ [27].

The main difficulty for our approach in investigating a deeper Kondo regime in the Coulomb valleys stems from the very low voltage bias needed to probe energy scales that are exponentially suppressed in $\delta E(n_g)$ as T_K. Indeed, finite-size effects limit the resolution in eV_b that we can achieve and hinder the observation of Kondo physics at small coupling or deep in the Coulomb valleys. Hence, our method is complementary to NRG: while the latter is more suited for studying the universal features of relevant low-energy approximations, our approach allows for a more direct comparison with experiments that have to cope with the interplay and possible competition between different energy scales.

In the Supplemental Material [27], we show the robustness of the TKE features against coupling anisotropies and the TKE disappearance when the MZMs acquire an energy splitting.

Conclusions. We analyzed the out-of-equilibrium properties of a minimal model for the topological Kondo effect, aiming at a microscopic description alternative to RG approaches and a qualitative understanding of transport signatures that may arise in double nanowire experiments. Our results present evidence of the onset of strongly correlated states compatible with a crossover between a weak-coupling and a topological Kondo regime.

First, the charge and the effective magnetization of the Majorana Cooper-pair box are characterized by different relaxation behaviors: the former only depends on the system-leads hybridization Γ, whereas the latter presents two separate timescales. In analogy with the dynamical features of the Anderson impurity model, we used the longer timescale to estimate the Kondo temperature associated with the TKE, with results compatible with the RG predictions [4,6].

Second, the nonlocal conductance in the intermediate- to strong-coupling regimes matches the predicted value

$G_{\mathrm{TKE}} = 2G_0/M$ at the charge degeneracy point, where T_K is the largest. In the Coulomb valleys, it presents large deviations from the noninteracting resonant level approximation that well describes the weak-coupling regime and two-terminal devices [17]. When the resonant level approximation fails, the conductance displays a plateau in the Coulomb valleys, hinting at a crossover to the topological Kondo regime.

Our results are obtained through an MPS approach that allows for the study of topological Kondo models without recurring to perturbation theory in the Majorana-lead coupling or requiring any particular hierarchy of the involved energy scales as expected in realistic devices [19]. It is therefore well suited to understand the crossover between strong- and weak-coupling regimes as well as the corrections to the RG predictions on the TKE when we probe the system at energy scales comparable with T_K.

Our method can be extended to more complex topological Kondo models, including the coupling of Majorana modes [9] caused by crossed-Andreev and cotunneling processes, the generalization to multichannel topological systems, and the presence of spurious quantum dots in the devices, which may cause additional Kondo effects [50–54]. This approach can be applied to the transport features of many strongly interacting nanodevices based on quantum dots coupled to superconducting islands [55–58]. Our method can be extended to more complex topological Kondo models, including the coupling of Majorana modes [9] caused by crossed-Andreev and cotunneling processes, the generalization to multichannel topological systems, and the presence of spurious quantum dots in the devices, which may cause additional Kondo effects [50–54]. This approach can be applied to the transport features of many strongly interacting nanodevices based on quantum dots coupled to superconducting islands [55–58].

Acknowledgments. We thank F. Buccheri, R. Egger, and J. Paaske for insightful discussions. M.W., L.M., and M.B. are supported by the Villum Foundation (Research Grant No. 25310). C.-M.C. acknowledges the support by the Ministry of Science and Technology (MOST) under Grant No. 111-2112-M-110-006-MY3, and by the Yushan Young Scholar Program under the Ministry of Education (MOE) in Taiwan. This project has received funding from the European Union's Horizon 2020 research and innovation program under the Marie Sklodowska-Curie Grant Agreement No. 847523 "INTERACTIONS." This work was supported by Q@TN, the joint laboratory between University of Trento, FBK–Fondazione Bruno Kessler, INFN–National Institute for Nuclear Physics, and CNR–National Research Council.

[1] E. Prada, P. San-Jose, M. W. de Moor, A. Geresdi, E. J. Lee, J. Klinovaja, D. Loss, J. Nygård, R. Aguado, and L. P. Kouwenhoven, From Andreev to Majorana bound states in hybrid superconductor-semiconductor nanowires, Nat. Rev. Phys. **2**, 575 (2020).

[2] C. W. J. Beenakker, Search for non-Abelian Majorana braiding statistics in superconductors, SciPost Phys. Lect. Notes 15 (2020).

[3] K. Flensberg, F. von Oppen, and A. Stern, Engineered platforms for topological superconductivity and Majorana zero modes, Nat. Rev. Mater. **6**, 944 (2021).

[4] B. Béri and N. R. Cooper, Topological Kondo effect with Majorana fermions, Phys. Rev. Lett. **109**, 156803 (2012).

[5] B. Béri, Majorana-Klein hybridization in topological superconductor junctions, Phys. Rev. Lett. **110**, 216803 (2013).

[6] A. Altland and R. Egger, Multiterminal Coulomb-Majorana junction, Phys. Rev. Lett. **110**, 196401 (2013).

[7] D. Liu, Z. Cao, X. Liu, H. Zhang, and D. E. Liu, Topological Kondo device for distinguishing quasi-Majorana and Majorana signatures, Phys. Rev. B **104**, 205125 (2021).

[8] K. Michaeli, L. A. Landau, E. Sela, and L. Fu, Electron teleportation and statistical transmutation in multiterminal Majorana islands, Phys. Rev. B **96**, 205403 (2017).

[9] A. Altland, B. Béri, R. Egger, and A. M. Tsvelik, Multichannel Kondo impurity dynamics in a Majorana device, Phys. Rev. Lett. **113**, 076401 (2014).

[10] M. R. Galpin, A. K. Mitchell, J. Temaismithi, D. E. Logan, B. Béri, and N. R. Cooper, Conductance fingerprint of Majorana fermions in the topological Kondo effect, Phys. Rev. B **89**, 045143 (2014).

[11] L. Herviou, K. Le Hur, and C. Mora, Many-terminal Majorana island: From topological to multichannel Kondo model, Phys. Rev. B **94**, 235102 (2016).

[12] F. Buccheri, A. Nava, R. Egger, P. Sodano, and D. Giuliano, Violation of the Wiedemann-Franz law in the topological Kondo model, Phys. Rev. B **105**, L081403 (2022).

[13] A. Altland, B. Béri, R. Egger, and A. M. Tsvelik, Bethe ansatz solution of the topological Kondo model, J. Phys. A: Math. Theor. **47**, 265001 (2014).

[14] F. Buccheri, H. Babujian, V. E. Korepin, P. Sodano, and A. Trombettoni, Thermodynamics of the topological Kondo model, Nucl. Phys. B **896**, 52 (2015).

[15] B. Béri, Exact nonequilibrium transport in the topological Kondo effect, Phys. Rev. Lett. **119**, 027701 (2017).

[16] M. Papaj, Z. Zhu, and L. Fu, Multichannel charge Kondo effect and non-Fermi-liquid fixed points in conventional and topological superconductor islands, Phys. Rev. B **99**, 014512 (2019).

[17] C.-M. Chung, M. M. Wauters, and M. Burrello, Matrix product state simulations of quantum quenches and transport in Coulomb blockaded superconducting devices, Phys. Rev. B **106**, 094308 (2022).

[18] T. Kanne, D. Olsteins, M. Marnauza, A. Vekris, J. C. Estrada Saldaña, S. Loric, R. D. Schlosser, D. Ross, S. Csonka, K. Grove-Rasmussen, and J. Nygård, Double nanowires for hybrid quantum devices, Adv. Funct. Mater. **32**, 2107926 (2022).

[19] A. Vekris, J. C. Estrada Saldaña, T. Kanne, T. Hvid-Olsen, M. Marnauza, D. Olsteins, M. M. Wauters, M. Burrello, J. Nygård, and K. Grove-Rasmussen, Electronic transport in double-nanowire superconducting islands with multiple terminals, Nano Lett. **22**, 5765 (2022).

[20] Y. Oreg, G. Refael, and F. von Oppen, Helical liquids and Majorana bound states in quantum wires, Phys. Rev. Lett. **105**, 177002 (2010).

[21] R. M. Lutchyn, J. D. Sau, and S. Das Sarma, Majorana fermions and a topological phase transition in semiconductor-superconductor heterostructures, Phys. Rev. Lett. **105**, 077001 (2010).

[22] K. Grove-Rasmussen, G. Steffensen, A. Jellinggaard, M. H. Madsen, R. Žitko, J. Paaske, and J. Nygård, Yu-Shiba-Rusinov screening of spins in double quantum dots, Nat. Commun. **9**, 2376 (2018).

[23] S. Vaitiekėnas, R. S. Souto, Y. Liu, P. Krogstrup, K. Flensberg, M. Leijnse, and C. M. Marcus, Evidence for spin-polarized bound states in semiconductor–superconductor–ferromagnetic-insulator islands, Phys. Rev. B **105**, L041304 (2022).

[24] R. S. Souto, M. M. Wauters, K. Flensberg, M. Leijnse, and M. Burrello, Multiterminal transport spectroscopy of subgap states in Coulomb-blockaded superconductors, Phys. Rev. B **106**, 235425 (2022).

[25] B. van Heck, A. R. Akhmerov, F. Hassler, M. Burrello, and C. W. J. Beenakker, Coulomb-assisted braiding of Majorana fermions in a Josephson junction array, New J. Phys. **14**, 035019 (2012).

[26] S. Plugge, A. Rasmussen, R. Egger, and K. Flensberg, Majorana box qubits, New J. Phys. **19**, 012001 (2017).

[27] See Supplemental Material at http://link.aps.org/supplemental/10.1103/PhysRevB.108.L220302 for further data and technical details, which also includes Refs. [61–67].

[28] K. G. Wilson, The renormalization group: Critical phenomena and the Kondo problem, Rev. Mod. Phys. **47**, 773 (1975).

[29] L. G. G. V. Dias da Silva, F. Heidrich-Meisner, A. E. Feiguin, C. A. Büsser, G. B. Martins, E. V. Anda, and E. Dagotto, Transport properties and Kondo correlations in nanostructures: Time-dependent DMRG method applied to quantum dots coupled to Wilson chains, Phys. Rev. B **78**, 195317 (2008).

[30] M. M. Wauters, C.-M. Chung, L. Maffi, and M. Burrello, Simulations of the dynamics of quantum impurity problems with matrix product states, arXiv:2304.13756 [cond-mat.str-el] (2023).

[31] A. Keselman, C. Murthy, B. van Heck, and B. Bauer, Spectral response of Josephson junctions with low-energy quasiparticles, SciPost Phys. **7**, 50 (2019).

[32] J. Haegeman, J. I. Cirac, T. J. Osborne, I. Pižorn, H. Verschelde, and F. Verstraete, Time-dependent variational principle for quantum lattices, Phys. Rev. Lett. **107**, 070601 (2011).

[33] J. Haegeman, C. Lubich, I. Oseledets, B. Vandereycken, and F. Verstraete, Unifying time evolution and optimization with matrix product states, Phys. Rev. B **94**, 165116 (2016).

[34] M. Yang and S. R. White, Time-dependent variational principle with ancillary Krylov subspace, Phys. Rev. B **102**, 094315 (2020).

[35] M. Fishman, S. R. White, and E. M. Stoudenmire, The ITensor software library for tensor network calculations, SciPost Phys. Codebases 4 (2022).

[36] The source code can be found in the repository https://github.com/chiamin/QuenchTranportTwoChains.

[37] D. Lobaskin and S. Kehrein, Crossover from nonequilibrium to equilibrium behavior in the time-dependent Kondo model, Phys. Rev. B **71**, 193303 (2005).

[38] F. B. Anders and A. Schiller, Real-time dynamics in quantum-impurity systems: A time-dependent numerical renormalization-group approach, Phys. Rev. Lett. **95**, 196801 (2005).

[39] M. F. Cavalcante, R. G. Pereira, and M. C. O. Aguiar, Quench dynamics of the Kondo effect: Transport across an impurity coupled to interacting wires, Phys. Rev. B **107**, 075110 (2023).

[40] E. H. Lieb and D. W. Robinson, The finite group velocity of quantum spin systems, Commun. Math. Phys. **28**, 251 (1972).

[41] L. Bonnes, F. H. L. Essler, and A. M. Läuchli, "Light-cone" dynamics after quantum quenches in spin chains, Phys. Rev. Lett. **113**, 187203 (2014).

[42] B. Bertini, M. Collura, J. De Nardis, and M. Fagotti, Transport in out-of-equilibrium XXZ chains: Exact profiles of charges and currents, Phys. Rev. Lett. **117**, 207201 (2016).

[43] J. Viti, J.-M. Stéphan, J. Dubail, and M. Haque, Inhomogeneous quenches in a free fermionic chain: Exact results, Europhys. Lett. **115**, 40011 (2016).

[44] F. H. L. Essler and M. Fagotti, Quench dynamics and relaxation in isolated integrable quantum spin chains, J. Stat. Mech.: Theory Exp. (2016) 064002.

[45] M. Ljubotina, S. Sotiriadis, and T. Prosen, Non-equilibrium quantum transport in presence of a defect: The non-interacting case, SciPost Phys. **6**, 004 (2019).

[46] J. I. Väyrynen, A. E. Feiguin, and R. M. Lutchyn, Signatures of topological ground state degeneracy in Majorana islands, Phys. Rev. Res. **2**, 043228 (2020).

[47] The simulations with $M = 3$ are performed by setting $J_2 = 0$.

[48] Z. He and A. J. Millis, Entanglement entropy and computational complexity of the Anderson impurity model out of equilibrium: Quench dynamics, Phys. Rev. B **96**, 085107 (2017).

[49] A. Zazunov, A. Altland, and R. Egger, Transport properties of the Coulomb-Majorana junction, New J. Phys. **16**, 015010 (2014).

[50] M. Cheng, M. Becker, B. Bauer, and R. M. Lutchyn, Interplay between Kondo and Majorana interactions in quantum dots, Phys. Rev. X **4**, 031051 (2014).

[51] R. López, M. Lee, L. Serra, and J. S. Lim, Thermoelectrical detection of Majorana states, Phys. Rev. B **89**, 205418 (2014).

[52] J. F. Silva, L. G. G. V. D. da Silva, and E. Vernek, Robustness of the Kondo effect in a quantum dot coupled to Majorana zero modes, Phys. Rev. B **101**, 075428 (2020).

[53] I. Weymann, K. P. Wójcik, and P. Majek, Majorana-Kondo interplay in T-shaped double quantum dots, Phys. Rev. B **101**, 235404 (2020).

[54] A. E. Svetogorov, D. Loss, and J. Klinovaja, Enhancement of the Kondo effect in a quantum dot formed in a full-shell nanowire, Phys. Rev. B **107**, 134505 (2023).

[55] C.-X. Liu, G. Wang, T. Dvir, and M. Wimmer, Tunable superconducting coupling of quantum dots via Andreev bound states in semiconductor-superconductor nanowires, Phys. Rev. Lett. **129**, 267701 (2022).

[56] A. Tsintzis, R. S. Souto, and M. Leijnse, Creating and detecting poor man's Majorana bound states in interacting quantum dots, Phys. Rev. B **106**, L201404 (2022).

[57] T. Dvir, G. Wang, N. van Loo, C.-X. Liu, G. P. Mazur, A. Bordin, S. L. D. Ten Haaf, J.-Y. Wang, D. van Driel, F. Zatelli, X. Li, F. K. Malinowski, S. Gazibegovic, G. Badawy, E. P. A. M. Bakkers, M. Wimmer, and L. P. Kouwenhoven, Realization of a minimal Kitaev chain in coupled quantum dots, Nature (London) **614**, 445 (2023).

[58] A. Tsintzis, R. S. Souto, K. Flensberg, J. Danon, and M. Leijnse, Roadmap towards Majorana qubits and nonabelian physics in quantum dot-based minimal Kitaev chains, arXiv:2306.16289 [cond-mat.mes-hall] (2023).

[59] I. Affleck and D. Giuliano, Topological superconductor–Luttinger liquid junctions, J. Stat. Mech.: Theory Exp. (2013) P06011.

[60] G. Li, Y. Oreg, and J. I. Väyrynen, Multichannel topological Kondo effect, Phys. Rev. Lett. **130**, 066302 (2023).

[61] D. Sticlet, C. Bena, and P. Simon, Spin and Majorana polarization in topological superconducting wires, Phys. Rev. Lett. **108**, 096802 (2012).

[62] M. Kjaergaard, K. Wölms, and K. Flensberg, Majorana fermions in superconducting nanowires without spin-orbit coupling, Phys. Rev. B **85**, 020503(R) (2012).

[63] M. M. Rams and M. Zwolak, Breaking the entanglement barrier: Tensor network simulation of quantum transport, Phys. Rev. Lett. **124**, 137701 (2020).

[64] B. van Heck, R. M. Lutchyn, and L. I. Glazman, Conductance of a proximitized nanowire in the Coulomb blockade regime, Phys. Rev. B **93**, 235431 (2016).

[65] M. Yoshida, M. A. Whitaker, and L. N. Oliveira, Renormalization-group calculation of excitation properties for impurity models, Phys. Rev. B **41**, 9403 (1990).

[66] I. Affleck, A current algebra approach to the Kondo effect, Nucl. Phys. B **336**, 517 (1990).

[67] I. Affleck and A. W. W. Ludwig, Critical theory of overscreened Kondo fixed points, Nucl. Phys. B **360**, 641 (1991).